A cross-correlation objective function for least-squares migration and visco-acoustic imaging

Gaurav Dutta, Mrinal Sinha, and Gerard T. Schuster, King Abdullah University of Science and Technology*

SUMMARY

Conventional acoustic least-squares migration inverts for a reflectivity image that best matches the amplitudes of the observed data. However, for field data applications, it is not easy to match the recorded amplitudes because of the visco-elastic nature of the earth and inaccuracies in the estimation of source signature and strength at different shot locations. To relax the requirement for strong amplitude matching of least-squares migration, we use a normalized cross-correlation objective function that is only sensitive to the similarity between the predicted and the observed data. Such a normalized cross-correlation objective function is also equivalent to a time-domain phase inversion method where the main emphasis is only on matching the phase of the data rather than the amplitude. Numerical tests on synthetic and field data show that such an objective function can be used as an alternative to visco-acoustic least-squares reverse time migration (Q_p-LSRTM) when there is strong attenuation in the subsurface and the estimation of the attenuation parameter Q_p is insufficiently accurate.

INTRODUCTION

Least-squares migration (LSM) has been shown to produce images with balanced amplitudes, better resolution and fewer artifacts than standard migration (Lailly, 1984; Schuster, 1993; Nemeth et al., 1999; Duquet et al., 2000; Tang, 2009; Dai and Schuster, 2010; Dai et al., 2010; Wong et al., 2011; Huang and Schuster, 2012; Zhang et al., 2013). The improvements in the image quality from LSM are obtained by matching the amplitudes and phases of the predicted and the observed data under the Born approximation.

The standard implementation of LSM relies on using the L2 norm of the difference between the predicted and the observed data as the objective function. This implementation strongly emphasizes the matching of the amplitudes and the phases of the predicted and observed data. However, for real data, it is not easy to match the amplitudes directly because of the following factors (Dong et al., 2012; Zhang et al., 2013):

- The real earth is visco-elastic and the amplitudes and the phases of the propagating seismic waves get severely distorted. To mimic such an effect, visco-elastic simulations are required which are computationally very expensive. Also, estimation of the attenuation parameter, Q_p, is difficult.
- The earth is often assumed to be a constant density medium but in reality, density variations strongly affect the amplitudes of the reflected seismic signals. Hence matching the amplitudes of the predicted and the observed data under the acoustic assumption is not straightforward.
- In many cases, it is difficult to find a good estimate of the source signature, and the source strength varies at different shot locations.
- For long wavelengths, the amplitudes of the synthetic data do not match those of the real data because of the inherent limitations in numerical modeling.

In this paper, the objective function for least-squares migration is formulated as a similarity measure between the predicted and the observed data. A normalized zero lag cross-correlation objective function is used that relaxes the amplitude matching criterion of standard LSM and emphasizes the phase-mismatch between the Born-simulated data and the observed data. Such an implementation is equivalent to a time-domain phase inversion method where the phase spectra of the observed data are matched with that of the calculated data (Schuster, 1991; Sun and Schuster, 1993; Routh et al., 2011; Zhang et al., 2013). Numerical tests on synthetic and field data show that the inverted images obtained from using a zero-lag cross-correlation objective function are very similar to the ones obtained from using the conventional L2 norm misfit function. However, improvements in the image quality can be seen in the former case when the recorded data have strong attenuation. The reflector amplitudes below the high attenuative layers are better balanced because a zero-lag cross-correlation objective function emphasizes only the phase-mismatch rather than on the amplitude mismatch. A disadvantage of this method is that the true amplitudes of the reflectors are not preserved in the inverted images.

THEORY

For a given source, s, and receiver, g, the similarity between the predicted data, $p_{g,s}$, and observed data, $d_{g,s}$, can be expressed by their zero-lag cross-correlation. A normalized cross-correlation objective function can be written as (Routh et al., 2011; Zhang et al., 2013)

$$\varepsilon = -\sum_{s=1}^{ns}\sum_{g=1}^{ng} \frac{p_{g,s}}{||p_{g,s}||}.\frac{d_{g,s}}{||d_{g,s}||}, = -\sum_{s=1}^{ns}\sum_{g=1}^{ng} \hat{p}_{g,s}.\hat{d}_{g,s}, \quad (1)$$

where

$$\hat{p}_{g,s} = \frac{p_{g,s}}{||p_{g,s}||} = \text{ Normalized predicted data,}$$

$$\hat{d}_{g,s} = \frac{d_{g,s}}{||d_{g,s}||} = \text{ Normalized observed data.}$$

It is evident from equation 1 that when the predicted and observed traces are equal, their normalized cross-correlation has a minimum value of -1 while in all other cases it is between 0 and -1.

The gradient of the misfit function can be obtained by taking the Frechet derivative of equation 1 with respect to the pertur-

DOI http://dx.doi.org/10.1190/segam2014-1376.1

bation, $m(\mathbf{x})$, as

$$\frac{\partial \varepsilon}{\partial m} = \sum_{s=1}^{ns}\sum_{g=1}^{ng}\left[-\frac{1}{||p_{g,s}||}\frac{\partial p_{g,s}}{\partial m}.\hat{d}_{g,s} + \left(\hat{p}_{g,s}.\hat{d}_{g,s}\right)\frac{\partial}{\partial m}\left(\frac{-1}{||p_{g,s}||}\right)\right]$$

$$= \sum_{s=1}^{ns}\sum_{g=1}^{ng}\left[-\frac{1}{||p_{g,s}||}\frac{\partial p_{g,s}}{\partial m}.\hat{d}_{g,s} + \frac{1}{||p_{g,s}||^2}\frac{\partial p_{g,s}}{\partial m}.p_{g,s}\left(\hat{p}_{g,s}.\hat{d}_{g,s}\right)\right]$$

$$= \sum_{s=1}^{ns}\sum_{g=1}^{ng}\left[\frac{\partial p_{g,s}}{\partial m}.\underbrace{\frac{1}{||p_{g,s}||}\left\{\hat{p}_{g,s}\left(\hat{p}_{g,s}.\hat{d}_{g,s}\right)-\hat{d}_{g,s}\right\}}_{\text{weighted residual trace}}\right] \quad (2)$$

The predicted trace, $p_{g,s}$, in this case is scaled by its normalized dot-product with the observed trace, $d_{g,s}$. Such a scaling controls the amplitude of the predicted trace according to the similarity between the observed and the predicted traces.

Numerically, the gradient here is computed by taking a zero-lag cross-correlation of the forward propagated source wavefield and the backward propagated weighted residual seismogram given in equation 2. This is also equivalent to a time-domain phase inversion method (Schuster, 1991; Sun and Schuster, 1993; Zhang et al., 2013) where at every iteration of the inversion, the phase mismatch between the predicted and the observed traces are minimized.

Mathematically, the L2 norm objective function is equivalent to the zero-lag cross-correlation objective function. It differs only in terms of the gradient computation. The gradient of the L2 norm objective function for standard LSM can be expressed as

$$\frac{\partial \varepsilon}{\partial m} = \sum_{s=1}^{ns}\sum_{g=1}^{ng}\frac{\partial p_{g,s}}{\partial m}.\underbrace{\left(p_{g,s}-d_{g,s}\right)}_{\text{residual trace}}. \quad (3)$$

The gradient in this case is computed by taking a zero-lag cross-correlation of the forward propagated source wavefield and the backward propagated residual wavefield. The gradient of the cross-correlation norm in equation 2 is similar to the gradient of the L2 norm objective function in equation 3 except that in the former case, the predicted trace is scaled by its weighted dot product with the observed trace.

The following steps are carried out for numerically implementing LSM using the cross-correlation objective function by a preconditioned conjugate gradient method, where a diagonal preconditioning matrix $\mathbf{C}$ is assumed.

- Form the misfit function, ε, given by equation 1.
- Compute the gradient, $\mathbf{gk}^{(i+1)}$ at the $i+1$-th iteration using equation 2.
- Update the gradient using the conjugate gradient formula as

  $$\mathbf{dk}^{(i+1)} = \mathbf{C}\mathbf{gk}^{(i+1)} + \beta\mathbf{dk}^{(i)},$$

  where β is given by

  $$\beta = \frac{\left(\mathbf{gk}^{(i+1)}\right)^T\mathbf{C}\mathbf{gk}^{(i+1)}}{\left(\mathbf{gk}^{(i)}\right)^T\mathbf{C}\mathbf{gk}^{(i)}}.$$

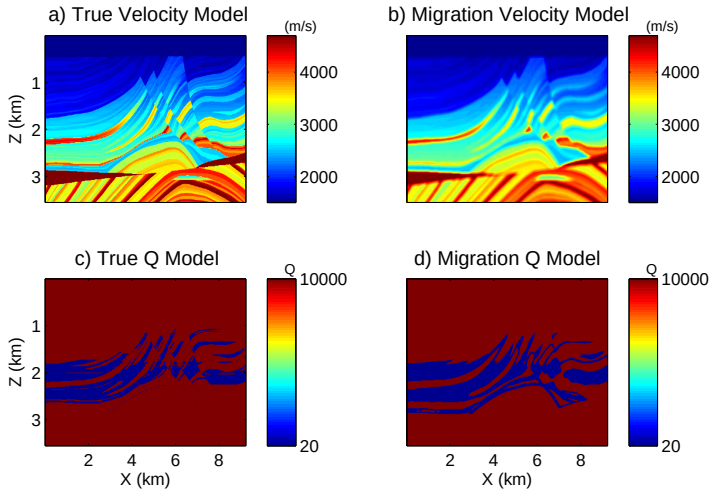

Figure 1: The modified Marmousi model: a) true velocity model, b) migration velocity model, c) true Q_p model, and d) migration Q_P model used for Q_p -LSRTM

- Compute the step length α as

  $$\alpha = \frac{\left(\mathbf{dk}^{(i+1)}\right)^T\mathbf{gk}^{(i+1)}}{\left(\mathbf{Ldk}^{(i+1)}\right)^T\left(\mathbf{Ldk}^{(i+1)}\right)},$$

  where $\mathbf{L}$ represents a Born modeling operator.
- Update the reflectivity image,

  $$\mathbf{m}^{(i+1)} = \mathbf{m}^{(i)} + \alpha\mathbf{dk}^{(i+1)}.$$

NUMERICAL EXAMPLES

The phase-inversion LSM method is now tested on the Marmousi model with strong subsurface attenuation. Figures 1(a) and 1(c) show the true velocity and Q_p models, respectively, used for generating the observed data with attenuation. The migration velocity model is shown in Figure 1(b) and the migration Q_p model used for Q_p-LSRTM (Dutta et al., 2013) is shown in Figure 1(d). The Q_p model is chosen such that the attenuation layers are overlying the targeted deeper anticlines. The observed synthetic data are generated with a 2-8 time-space domain staggered-grid finite-difference visco-acoustic modeling code. A fixed spread acquisition geometry is used where 200 shots are excited with a 40 m shot interval at a depth of 10 m. Each shot is recorded with 400 receivers and a 20 m receiver interval with a recording time of around 8 s.

Conventional acoustic reverse time migration (RTM) and least-squares reverse time migration (LSRTM) images using the L2 norm objective function are shown in Figures 2(a)-2(b), respectively. The LSRTM image shows better resolution and fewer artifacts than the RTM image in the shallow layers but in the deeper layers, the amplitudes of the images from these two methods are very weak. The reflectors below the anticlines cannot be properly delineated in spite of using a very accurate velocity model for migration.

DOI http://dx.doi.org/10.1190/segam2014-1376.1

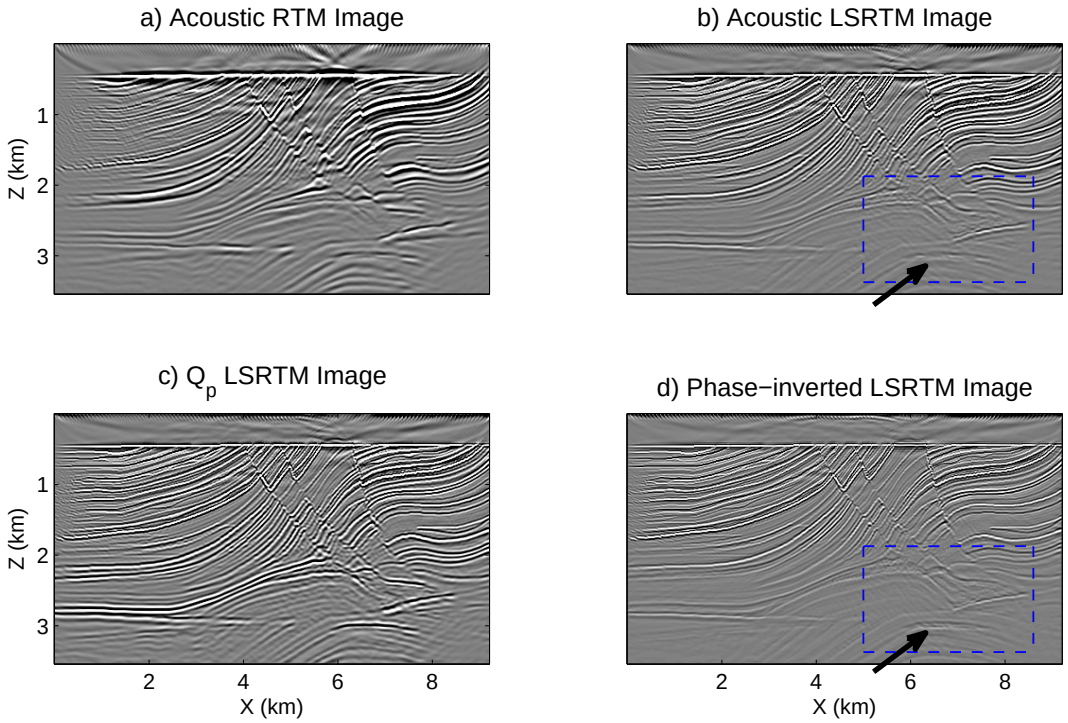

Figure 2: Comparison between images from a) acoustic RTM, b) acoustic LSRTM, c) Q_p-LSRTM, and d) phase-inverted LSRTM. The blue boxes highlight the areas where improvements in the image quality can be seen from phase-inverted LSM.

The Q_p-LSRTM image, shown in Figure 2(c), shows significant improvements in the image quality in the shallow and deeper parts. However, Q_p-LSRTM is computationally expensive and it requires an estimate of the smoothly varying Q_p distribution in the subsurface. For surface seismic data, estimation of Q_p is difficult and in most cases, the estimation is ambiguous. The acoustic phase-inverted LSRTM image, shown in Figure 2(d), shows some improvements over the acoustic LSRTM image in Figure 2(b). The zoom view of the blue boxes in Figure 2 are shown in Figure 3 where the improvements in the image quality from phase-inverted LSM are highlighted. The target reservoir, indicated by the black arrow in Figure 3, is better delineated in the phase-inverted LSM image. This happens because the normalized cross-correlation objectives ignores the effect of amplitudes and emphasizes only matching the phase of the predicted and the observed data. Hence, the deeper layers, whose reflection amplitudes are very weak in the observed data, are imaged with better balanced amplitudes.

The phase inversion method is also tested on a marine data set from the Gulf of Mexico (GoM). There are 515 shots fired at a shot interval of 37.5 m. Each shot is recorded by 480 receivers spread at an interval of 12.5 m. The velocity tomogram, shown in Figure 4, is used as the migration velocity model. The RTM and LSRTM images using the L2 norm and the cross-correlation objective functions after 20 iterations are shown in Figure 5 and their zoom views are compared in Figure 6. Compared to the standard LSRTM image, the phase-inverted LSRTM image shows modest improvements in the shallow

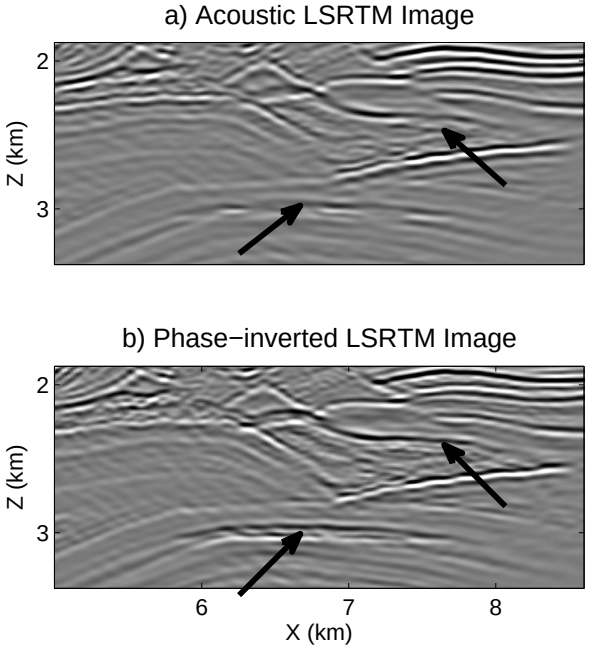

Figure 3: Zoom views of the blue boxes in Figure 2. The black arrows point to the areas where noticeable improvements in the image can be seen. Both these figures are plotted to the same scale.

DOI http://dx.doi.org/10.1190/segam2014-1376.1

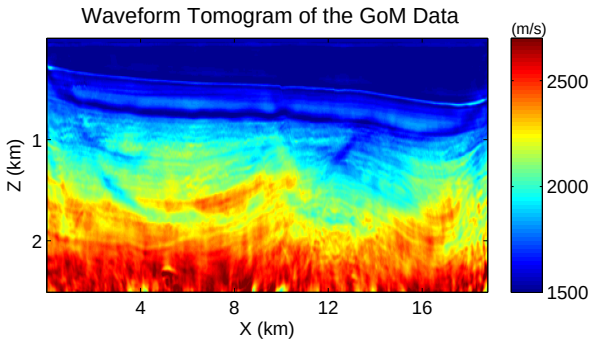

Figure 4: Velocity model of the GoM data obtained by waveform inversion.

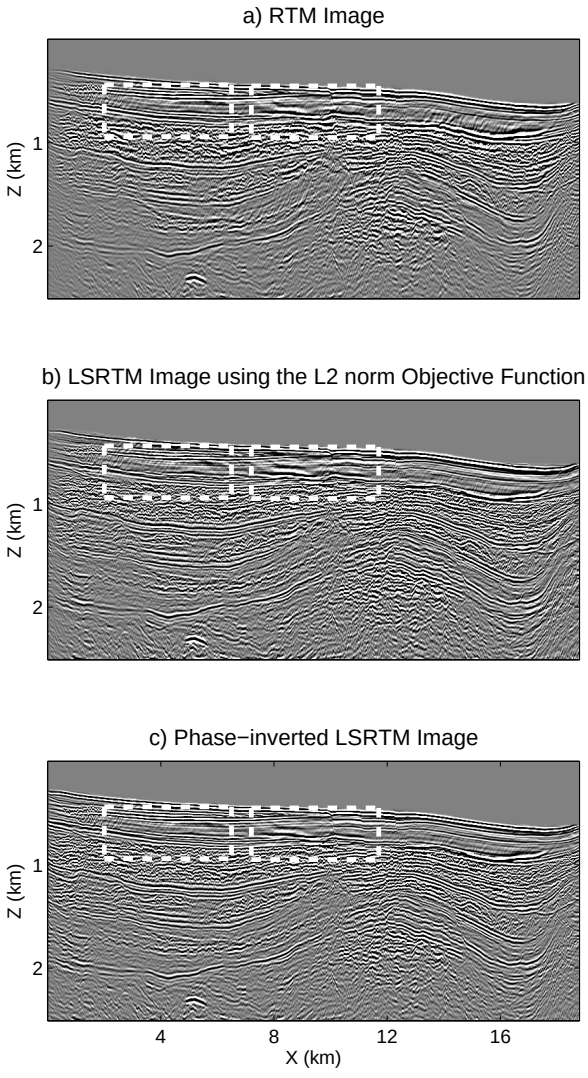

Figure 5: GoM field data example: a) RTM image, b) LSRTM image using the L2 norm objective function, and c) Phase-inverted LSRTM image.

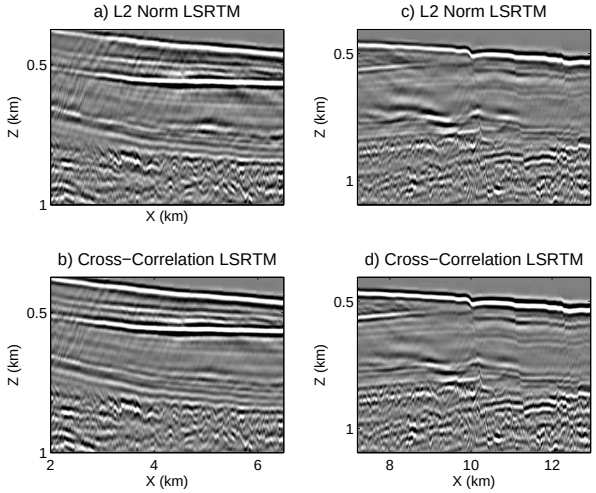

Figure 6: Zoom views of the dashed boxes in Figure 5. a) RTM image, b) LSRTM image using the L2 norm objective function, and c) phase-inverted LSRTM image. The strong diving artifacts that are present in the standard LSRTM images in a) and c) have been removed in the phase-inverted LSM image in b) and d).

layers. The strong diving-wave and head-wave artifacts, indicated by the dashed boxes in Figure 5 and in the zoom views in Figure 6, are eliminated in the phase-inverted LSM image. As a result, the faults in the shallow layers are better delineated. These artifacts are mitigated because the predicted data from them do not match in phase with the observed data and the cross-correlation objective function suppresses these dissimilar events. However, in the deeper parts, the images from both inversions are similar since the deeper layers are beyond the reach of the strong diving waves.

CONCLUSIONS

A time-domain phase inversion method for least squares migration is presented that emphasizes matching the phases of the observed and the predicted data and relaxes the amplitude matching criterion of standard least-squares migration. Numerical tests on synthetic and field data show that the inverted images using the L2 norm and the cross-correlation objective functions are similar when there is very little or no attenuation in the subsurface. However, if the recorded data have strong attenuation, then the cross-correlation objective function can be used as an alternative to visco-acoustic imaging during least-squares migration.

ACKNOWLEDGMENTS

We thank the sponsors of the Center for Subsurface Imaging and Modeling (CSIM) consortium for their support and KAUST Supercomputing Laboratory for providing the computational resources.

DOI http://dx.doi.org/10.1190/segam2014-1376.1

http://dx.doi.org/10.1190/segam2014-1376.1

EDITED REFERENCES

Note: This reference list is a copy-edited version of the reference list submitted by the author. Reference lists for the 2014 SEG Technical Program Expanded Abstracts have been copy edited so that references provided with the online metadata for each paper will achieve a high degree of linking to cited sources that appear on the Web.

REFERENCES

Dai, W., C. Boonyasiriwat, and G. T. Schuster, 2010, 3D multi-source least-squares reverse time migration: 80th Annual International Meeting, SEG, Expanded Abstracts, 3120–3124, http://dx.doi.org/10.1190/1.3513494.

Dai, W., and G. T. Schuster, 2010, Multi-source wave equation least-squares migration with a deblurring filter: 72nd Conference & Exhibition, EAGE, Extended Abstracts, P276.

Dong, S., J. Cai, M. Guo, S. Suh, Z. Zhang, B. Wang, and Z. Li, 2012, Least-squares reverse time migration: Towards true amplitude imaging and improving the resolution: 82nd Annual International Meeting, SEG, Expanded Abstracts, doi: 10.1190/segam2012-1488.1.

Duquet, B., K. J. Marfurt, and J. A. Dellinger, 2000, Kirchhoff modeling, inversion for reflectivity, and subsurface illumination: Geophysics, **65**, 1195–1209, http://dx.doi.org/10.1190/1.1444812.

Dutta, G., K. Lu, X. Wang, and G. T. Schuster, 2013, Attenuation compensation in least-squares reverse time migration using the visco-acoustic wave equation: 83rd Annual International Meeting, SEG, Expanded Abstracts, 3721–3725.

Huang, Y., and G. T. Schuster, 2012, Multisource least-squares migration of marine streamer data with frequency-division encoding: Geophysical Prospecting, **60**, no. 4, 663–680, http://dx.doi.org/10.1111/j.1365-2478.2012.01086.x.

Lailly, P., 1984, Migration methods: Partial but efficient solutions to the seismic inverse problem, *in* F. Santosa, ed., Inverse problems of acoustic and elastic waves: SIAM, 182–214.

Nemeth, T., C. Wu, and G. T. Schuster, 1999, Least-squares migration of incomplete reflection data: Geophysics, **64**, 208–221, http://dx.doi.org/10.1190/1.1444517.

Routh, P., J. Krebs, S. Lazaratos, A. Baumstein, I. Chikichev, S. Lee, N. Downey, D. Hinkley, and J. Anderson, 2011, Full-wavefield inversion of marine streamer data with the encoded simultaneous source method: 73rd Conference & Exhibition, EAGE, Extended Abstracts, F032.

Schuster, G., 1991, Wave equation phase inversion in the frequency domain: 61st Annual International Meeting, SEG, Expanded Abstracts, 909–912.

Schuster, G. T., 1993, Least-squares cross-well migration: 63rd Annual International Meeting, SEG, Expanded Abstracts, 110–113.

Sun, Y., and G. Schuster, 1993, Time domain phase inversion: 63rd Annual International Meeting, SEG, Expanded Abstracts, 684–687.

Tang, Y., 2009, Target-oriented wave-equation least-squares migration/inversion with phase-encoded Hessian: Geophysics, **74**, no. 6, WCA95–WCA107, http://dx.doi.org/10.1190/1.3204768.

Wong, M., S. Ronen, and B. Biondi, 2011, Least-squares reverse time migration/inversion for ocean bottom data: A case study: 81st Annual International Meeting, SEG, Expanded Abstracts, 2369–2373.

Zhang, Y., L. Duan, and Y. Xie, 2013, A stable and practical implementation of least-squares reverse time migration: 83rd Annual International Meeting, SEG, Expanded Abstracts, 3716–3720.